Translational Oncology 14 (2021) 100926

Contents lists available at ScienceDirect

Translational Oncology

journal homepage: www.elsevier.com/locate/tranon

Therapeutic potential of Fingolimod in triple negative breast cancer preclinical models

Tristan Rupp*, Océane Pelouin, Laurie Genest, Christophe Legrand, Guillaume Froget, Vincent Castagné

Porsolt SAS, ZA de Glatigné, 53940 Le Genest-Saint-Isle, France

ARTICLE INFO

Keywords:
Triple negative breast cancer
Preclinical models
Tumor progression
Metastasis
Fingolimod
Sphingosine-1-Phosphate

ABSTRACT

Surgery followed by a chemotherapy agent is the first-line treatment for breast cancer patients. Nevertheless, new targets are required for women with triple-negative breast cancer (TNBC) in order to improve the treatment of this aggressive cancer subtype. Multiple pro-inflammatory molecules including lipid-based substances such as sphingosine-1-phosphate (S1P) promote cancer progression. In this preclinical study, we aim to investigate the efficacy of Fingolimod, an inhibitor of S1P / S1P receptors axis, already approved as an immunomodulator in multiple sclerosis.

The impact of Fingolimod was analyzed using in vitro 2D and 3D cell survival analysis and in vivo orthotopic graft models, using mouse and human TNBC cells implanted in immunocompetent or immunodeficient mice, respectively. Resection of the tumor primary mass was also performed to mimic the clinical standard of care.

We demonstrated that Fingolimod repressed tumor cell survival in vitro. We also showed in preclinical mouse TNBC models that Fingolimod repressed tumor progression and liver and spleen metastases without apparent adverse effects on the animals. Our data indicate that Fingolimod induces tumor cells apoptosis and thereby represses tumor progression.

Globally, our data suggest that Fingolimod merits further evaluation as a potential therapeutic opportunity for TNBC.

Introduction

Breast cancer is an important public health concern affecting patient survival and quality of life. Advanced breast cancer remains difficult to treat due to aggressive cell spreading into other organs. The main organs colonized by metastasis are bone, lymph nodes, liver, lungs, and brain, strongly affecting the prognosis of patients with a median overall survival of 2–3 years [1]. Breast cancer is a heterogeneous disease with several histopathological forms and molecular subtypes, including specific genetic alterations including mutations, losses or amplifications of genes. Gene profiles of estrogen receptor (ER), progesterone receptor (PR), and human epidermal growth factor receptor 2 (HER2) serve as a basis for defining tailored therapeutic strategies. Four main subtypes of breast cancer are considered in clinical practice, e.g. triple negative breast cancers (TNBC; ER-, PR- and HER2-negative), HER2-positive breast cancers, and luminal A-like (ER-positive, PR-positive, and HER2-positive) or luminal B-like breast cancers (ER-low, PR-low, and HER2-negative or positive). While tumors expressing ER and/or PR are sensitive to anti-hormonal drugs and HER2-positive tumors are sensitive to EFGR-targeting, tumors not expressing ER, PR, and HER2 are poorly responsive to hormonal or EFGR-targeting strategies [2]. As a consequence, patients with TNBC have poor survival compared with non-TNBC patients [3].

Inflammatory-related molecules such as cytokines, chemokines, and cells, are involved in tumor initiation and cancer progression. Other mediators such as lipid-derived molecules have recently been associated with inflammatory diseases. There is growing evidence that one of the lipid-related inflammatory molecules, sphingosine-1-phosphate (S1P), contributes to inflammation, disease progression, and cancer [4]. S1P is generated by sphingosine kinase 1 and is secreted in the extracellular microenvironment. S1P activates dedicated receptors (S1PR) and is involved in multiple cellular processes such as cell survival, migration, angiogenesis, blood vessel maturation, and immune cell trafficking [5].

Abbreviations: EGFR, Epidermal Growth Factor Receptor; EMT, Epithelial-to-Mesenchymal Transition; ER, Estrogen Receptor; HER2, Epidermal Growth Factor Receptor 2; PR, Progesterone Receptor; Luc, Luciferase; RFP, Red Fluorescence Protein; S1P, Sphingosine-1-Phosphate; S1PR, Sphingosine-1-Phosphate Receptor; SD, Standard Deviation; TNBC, Triple Negative Breast Cancer.

* Corresponding author.
E-mail addresses: trupp@porsolt.com, rupptristan@hotmail.fr (T. Rupp).

https://doi.org/10.1016/j.tranon.2020.100926
Received 15 July 2020; Received in revised form 14 October 2020; Accepted 21 October 2020

S1P level is elevated in the plasma of patients with hepatocellular carcinoma [6,7] and biliary tract cancer [8]. Moreover, the S1P protein level is upregulated in breast cancer [9]. Another component of the S1P signaling, Sphingosine Kinase 1, is also upregulated in breast cancer tissue samples [10]. These elements therefore suggest a potential prognosis and therapeutic value of the S1P pathway in breast cancer.

Fingolimod is an FDA- and EMA-approved drug used for the treatment of multiple sclerosis. It retains T cells in secondary lymph organs, limiting their infiltration into the brain and delaying disease progression [11]. Fingolimod acts as an analogue of S1P and inhibits S1PRs including S1PR1 [12,13]. Recent studies suggest that Fingolimod may represent a relevant therapeutic strategy for cancer [13,14]. The efficacy of Fingolimod still needs to be demonstrated in human patients, however, several preclinical studies indicate its potential as a new anticancer treatment. Fingolimod represses in vivo tumor progression in different preclinical models such as colon cancer [15], liver cancer [16], and prostate cancer [17]. Moreover, Fingolimod can modulate the tumor microenvironment through the repression of tumor angiogenesis [18,19], which is a crucial mechanism driving tumor progression [20,21]. Fingolimod modulates important signaling pathways involved in cancer progression. including mTOR, PIK3/AKT, and MAPK/ERK signaling [14,22]. In breast cancer, Fingolimod reduces tumor progression in the JygMC(A) transgenic model [23], in the Walker 256 rat grafting model [24], and in an obesity-related breast cancer mouse model [25]. However, this same anti-tumor effect was not seen in other similar studies [26,27]. In view of these apparently contradictory data, the impact of Fingolimod in preclinical models needs clarification, including the identification of a sensitive-subtype of breast cancer.

Even though Fingolimod may be an interesting target for breast cancer, no clear analysis of the TNBC subtype is described so far using clinically-relevant models analyzing tumor progression and metastasis. Here, using in vitro and in vivo models, we examine the efficacy of Fingolimod treatment for breast cancer of the TNBC subtype. We demonstrated that Fingolimod induces TNBC cell death in vitro in a dose-dependent manner using 2D and 3D tumor models. In vivo, Fingolimod represses tumor growth and metastasis formation in liver and spleen in orthotopic TNBC models with or without tumor surgical resection. Moreover, Fingolimod does not induce obvious adverse side effects in the mouse. Our data indicate that Fingolimod merits further preclinical and clinical evaluation to halt tumor progression in TNBC.

Material and methods

Animals

6 week-old female BALB/cAnN-Foxn1nu/nu/Rj (= BALB/c-nude) mice or BALB/cJRj mice, supplied by Janvier Labs, were acclimated at least 5 days before the experiments. The implantation of tumor cells was performed on 7 or 8 week-old mice. BALB/cJRj mice were housed up 10 animals per cage in a biosafety level 1 laboratory. BALB/c-nude mice were housed in a biosafety level 2 laboratory and grouped up to 6 animals per individually ventilated cage (NEXGEN MOUSE IVC™, Allentown®) on NestPak® (Allentown®). Nesting enrichment was provided (tube, cotton, and wood). The laboratories were maintained under artificial lighting (12 h) between 7:00 and 19:00 in a controlled ambient temperature of 22 ± 2 °C, and relative humidity between 30 and 70%.

Cells and cell culture

4T1 triple negative mouse breast carcinoma (CRL-2539™ from ATCC®) and BT-20 triple negative human breast carcinoma cell line (ATCC HTB-19™ from ATCC®) were cultured in vitro according to Porsolt's specifications with RPMI 1640 (Gibco®, ATCC-formulated) supplemented with fetal bovine serum (FBS, Gibco®) at a final concentration of 10% and antibiotics (Penicillin 100 U/mL - Streptomycin 100 µg/mL, Gibco®) and were allowed to grow in a cell incubator at 37 °C and 5% CO_2. The MDA-MB-231-RFP-Luc triple negative breast adenocarcinoma cell line (SC041 from AMSBIO) expressing luciferase (Luc) and red fluorescence protein (RFP) was cultured following similar parameters, including 5 µg/mL of Blasticidin (Invivogen®, reference ant-bl-5b) in culture medium.

Before cell injection, 70–90% confluent cells were split and cell viability was assessed using an automated cell counter, Nucleocounter NC-200™ (Chemotec®). The cell suspension was prepared according to the viable cell count. All procedures were performed in aseptic conditions, under a laminar flow hood.

2D. culture cell viability assay

Cells were plated on 96-well plates (2000 cells/well with 3 to 4 replicates) for 24 h, before being treated with Cisplatin at 1.67, 16.7, and 167 µM [28,29] or Fingolimod at 0.01, 0.1, 1, 5, 10, 20, and 50 µM [17,30]. After 72 h of growth, MTS (3-(4,5-dimethylthiazol-2-yl)−5-(3-carboxymethoxyphenyl)−2-(4-sulfophenyl)−2H-tetrazolium, inner salt) incorporation assays were performed according to the manufacturer's instructions (CellTiter 96 aqueous non-radioactive cell proliferation assay, Promega®). Measured absorbance values at 490 nm, using a microplate reader Ensight™ (Perkin Elmer®), were normalized to the control vehicle-treated conditions as relative cell growth values.

3D. tumor spheroid assay

Cells were plated on 96-well plates (5000 cells/well with 7–8 replicates) in 96 well plate GravityPLUS™ Hanging Drop System (InSphero®) in culture medium for 48 h. Spontaneously formed tumor spheroids were treated with at 0.0167, 0.167, 1.67, 16.7, and 167 µM [28,29] or Fingolimod at 0.1, 1, 5, 10, 20, and 50 µM [17,30] in culture medium containing fluorescent DNA intercalating agent as marker of cell apoptosis and death (Sytox™ red Dead Cell Stain, Invitrogen™, #S34859). Cell confluence and positive area fluorescent cells were monitored by imaging using Ensight™ system (Perkin Elmer®) at 24 h and 96 h. Spheroid growth was determined by analyzing the total cell surface (in pixel^2). Cytotoxicity was determined by analyzing the plasma membrane integrity based on the incorporation of a fluorescent DNA intercalating agent that selectively stain cytolytic cells with compromised plasma membrane, as positive area in pixel^2 among the spheroid area (%).

Animal ethical consideration and limit points

All methods, designed to minimize animal suffering and to ensure good quality of biological samples, are adapted from basic procedures commonly used in studies performed in rodents. Experiments were conducted in strict accordance with Council Directive No. 2010/63/UE of September 22nd 2010 on the protection of animals used for scientific purposes, the French decree No. 2013–118 of February 1st 2013 on the protection of animals for use and care of laboratory animals, and with the recommendations of the Association for Assessment and Accreditation of Laboratory Animal Care (AAALAC). All experiments were also approved by the Internal Animal Care and Use Committee (IACUC) of Porsolt, for animal experimentation (Porsolt's agreement n °C5301 031).

Tumor volume and body weight of the animals were measured and recorded two to three times per week. Tumor volume exceeding 2000 mm^3, a weight loss greater than 20% relative to the initial weight of the animal, tumor necrosis including bleeding, ulceration, hypothermia (< 34 °C), dyspnea, failure to eat and drink, loss of balance, and marked sedation, were considered as critical limitation points. When one of these conditions was met, mice were sacrificed by CO_2 inhalation.

Orthotopic tumor in vivo murine model

5×10^5 4T1 cells or 5×10^6 MDA-MB-231-RFP-Luc cells were injected into the mammary fat pad. The cells to be implanted were resuspended in sterile PBS and kept on ice. Prior to surgery, mice were treated with Carprofen (Rimadyl™, reference RIM011) subcutaneously at 5 mg/kg, for pain prevention. Mice were then placed under anesthesia 2% isoflurane (Axience®, reference 152,678) at 2 L/min on a warming pad and with eye lubricant during the surgery. Mice were identified by permanent tattoo. The mice were injected with the cell suspension in the 4th left mammary fat gland. The belly of Balb/cJRj mice was shaved and the implanted area was cleaned with Chlorhexidine (Antisept™, reference ANT015). A small incision was made between the 4th left nipple and the median line. Tweezers were used to expose the mammary fat pad, identifiable by its white color. 50 µL of cell suspension was then injected into the mammary fat pad. Finally the mice were sutured and monitored (breathing) until they woke up.

Tumor volume was measured two to three times a week with a caliper, and tumor volume was calculated using the formula $V=(a2^*b)/2$, where b is the longest axis and a is the perpendicular axis to b.

Depending on the model used, primary tumors, lungs, livers, and spleens were collected. Whole tissues were rapidly removed, rinsed in physiological saline, dried on absorbent paper, and weighed.

For MDA-MB-231-RFP-Luc xenograft model, tumor growth was also monitored using in vivo bioluminescence imaging by measuring the luciferase activity expressed by the tumor cells. During the procedure animals were anesthetized, injected with D-luciferin (VivoGlo™, reference P1043) at 150 mg/mL i.p., and after 10 min imaged on an IVIS™ Lumina X5™ system (Perkin Elmer®), and maintained on a warm blanket. Measurements were acquired twice a week to track the dynamics of the tumor growth.

For MDA-MB-231-RFP-Luc xenograft model, potential lung metastasis formation was investigated using ex vivo fluorescence imaging via the measurement of the RFP signal expressed by tumor cells. Collected lungs were imaged for specific red fluorescent light (560/620 nm) on an IVIS™ Lumina X5™ system.

To quantify the bioluminescence and fluorescence signal, size-matched regions of interest (ROI) were obtained utilizing an automated method using Living Image™ software (version 4.7.1., Perkin Elmer®), and signals were quantified.

The metastasis index was calculated by the number of visible lung macro-metastases and was graded based on a scale of 1 metastatic foci - index 1; up to 5 metastatic foci - index 2; and more than 5 metastatic foci - index 3.

Survival was monitored each day and data was plotted into Kaplan-Meier graph.

Tumor resection in vivo murine model

Primary tumors were generated as indicated above. After 14 days, and prior to surgery, mice were treated with Carprofen (5 mg/kg). Mice were then placed under isoflurane anesthesia on a warm blanket and a small incision was made between the 4th left nipple and the median line. Tweezers were used to expose the tumors that were then removed using scissors. Finally the mice were sutured and monitored until they woke up.

Tumor volume was measured two to three times a week with a caliper.

Experimental metastasis in vivo murine model

2×10^6 MDA-MB-231-RFP-Luc cells were injected intravenously via the caudal vein using insulin syringe. The cells to be implanted were resuspended in sterile PBS and kept on ice. Mice were placed under anesthesia 2% isoflurane (Axience®, reference 152,678) at 2 L/min on a warming pad and with eye lubricant during the procedure. The tail of mice was cleaned with Chlorhexidine (Antisept™, reference ANT015) before the injection. Tumor cells were injected within a volume of 100 µL. Mice were identified by permanent tattoo. Finally the mice were monitored (breathing) until they woke up.

Lung metastasis formation was monitored using in vivo bioluminescence imaging by measuring the luciferase activity expressed by the tumor cells. During the procedure animals were anesthetized, injected with D-luciferin (VivoGlo™, reference P1043) at 150 mg/mL i.p., and after 10 min imaged on an IVIS™ Lumina X5™ system (Perkin Elmer®), and maintained on a warm blanket. Measurements were acquired once a week to track the dynamics of the metastasis formation. After 4 days, mice were randomized in the different groups based on their body weight and were monitored during 11 additional days.

Treatments evaluated in murine models

Cisplatin was purchased from Santa Cruz® (reference sc-200,896) and Fingolimod was purchased from Selleckchem® (reference S5002).

Once the tumors reached an approximate size of 100 to 150 mm^3 for the orthotopic models or once the metastasis signal reached 1×10^7 photon/second in the intravenous model, the mice were randomized based on their tumor volume or bioluminescence signal into groups of 6 mice for MDA-MB-231-RFP-Luc orthotopic xenograft, 8 to 9 mice for the intravenous metastasis model, and 3–4 mice or 8 mice for 4T1 syngeneic orthotopic graft model. Mice were treated with Cisplatin at 1 mg/kg (diluted in saline) [31,32], Fingolimod at 5 mg/kg (diluted in saline) [23,33]. Drugs or vehicle were administrated via the intraperitoneal route (i.p.) route, five times a week until the end of the experiment.

Statistics

In vitro experiments were performed at least three times independently using at least three biological replicates per experiment. The IC50 was calculated using four parameters nonlinear regression analysis. Statistical analysis and graphical representations were performed using GraphPad Prism (version 8). p values < 0.05 were considered as statistically significant (* $p < 0.05$; ** $p < 0.01$; *** $p < 0.001$; **** $p < 0.0001$). All data per group have been checked for normality using the D'Agostino-Pearson test. In case of a non-significant difference, a parametric test was used, and in case of a significant difference, a non-parametric test was performed.

For in vitro 2D cell viability, data was analyzed using a one-way ANOVA (groups as factor). In the case of a significant group effect, post-hoc Bonferroni's multiple comparisons tests (versus control) were performed. Experiments were repeated at least three times in triplicate with consistent results.

For in vitro 3D spheroid assay, data was analyzed using a two-way ANOVA (groups and days as factor). In the case of a significant group effect, post-hoc Bonferroni's multiple comparisons tests (versus control) were performed. Experiments were repeated two times with seven to eight with consistent results.

Body weight data was analyzed using a two-way ANOVA (groups and days as factors) with repeated measures on each day. In the case of a significant group and/or interaction effect, post-hoc Tukey's or Bonferroni's multiple comparisons tests (for each day) were performed. Each experimental group consisted of at least six mice (Figs. 3–6), except one experiment with at least three mice (Fig. S5).

Fluorescence signal, organ weight, and metastasis index data, were analyzed using a one-way ANOVA (groups as factor). In the case of a significant group effect, post-hoc Tukey's or Bonferroni's multiple comparisons tests (for each day) were performed.

The cumulative survival distribution, relapse-free survival and distant metastasis-free survival were constructed using the Kaplan-Meier method. Differences between survival curves were tested for significance with the log rank test.

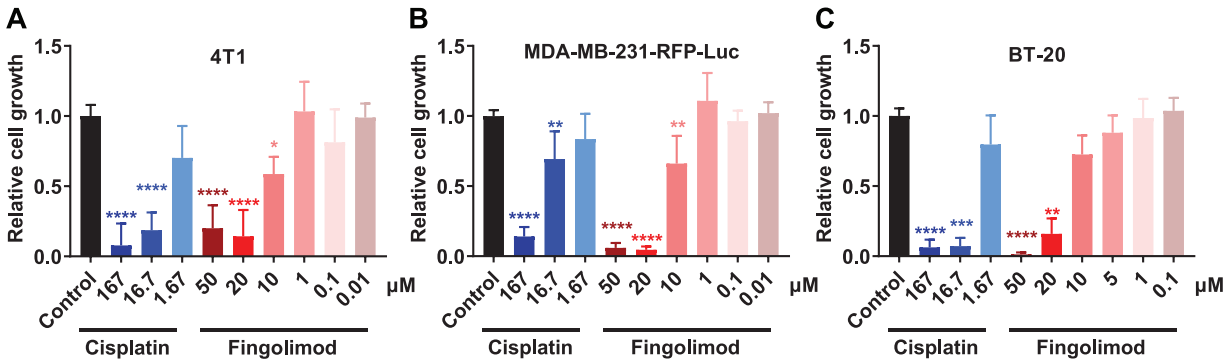

Fig. 1. Effects of Cisplatin and Fingolimod on TNBC in 2D cell viability assay.
A-C. Dose-response effect of Cisplatin and Fingolimod treatment on MDA-MB-231-RFP-Luc, 4T1, and BT20 TNBC using MTS incorporation cell viability assay. The study was performed with three to four replicates from three to five independent experiments. Data represent mean and SD. Statistical differences between the groups were determined using one-way ANOVA followed by Bonferroni's multiple comparisons test (vs. control, * $p \leq 0.05$, ** $p \leq 0.01$, *** $p \leq 0.001$, **** $p \leq 0.0001$).

Results

Fingolimod decreased in vitro TNBC cell viability in a dose-dependent manner

It has already been shown that S1P levels are upregulated in the serum of patients with breast cancer [34], suggesting that targeting of S1P axis might be of interest for therapy. Here, we used Fingolimod, an S1PRs inhibitor, and analyzed its effect on tumor cell viability. Fingolimod was compared to Cisplatin, a chemotherapy not currently used in standard therapy, but demonstrating renewed and potent interest in the treatment of TNBC clinical trials [35,36] and for preclinical research [28,37,38]. First, we investigated if and how Fingolimod affected cell viability in three cell lines, two human (BT20 and MDA-MB-231-RFP-Luc) and one mouse TNBC cancer cell lines (4T1), using an in vitro MTS incorporation assay. We demonstrated that Fingolimod dose-dependently reduced cell viability of the three TNBC cell lines (Fig. 1A-C and S1A-C). Cisplatin also induced reduced cell viability starting from a dose of 16.7 μM (Fig. 1A-C). The IC50 of Fingolimod was 11.27, 10.35, and 12.89 μM for 4T1, MDA-MB-231-RFP-Luc, and BT-20 cells, respectively (Fig. S1A-C).

In order to decipher how both compounds can affect cell viability, we developed a 3D culture model of tumor spheroid with the TNBC cell lines. The 3D tumor spheroid model has the advantage of mimicking the complexity and heterogeneity of tumors observed in patients [39,40]. The tumor microenvironment has several major characteristics, including hypoxic and nutriment gradients, structure and composition of the extracellular matrix, and cell–cell adhesion, which cannot be reproduced in a 2D monolayer cell culture [41]. We showed that MDA-MB-231 did not spontaneously form tumor spheroids after 48 h (Fig. S2), and could therefore not be used as in the 3D cellular model setting. Conversely, both BT20 and 4T1 cells generated tumor spheroids in identical culture conditions (Figs. S3 and S4). We demonstrated that Cisplatin significantly reduced the spheroid surface after 4 days of treatment starting from the dose of 1.67 μM for BT20. We also observed on day 1 a significant difference for the highest dose at 167 μM with BT20 cells (Fig. 2A). With 4T1 cells, Cisplatin reduced the spheroid size at all doses, despite an absence of significant difference for the highest dose at 167 μM (Fig. 2B). Moreover, Cisplatin significantly promoted cell apoptosis and necrosis at the dose of 167 μM on day 4 for BT20, but did not significantly affect 4T1 spheroids (Fig. 2C and 2D). Fingolimod significantly reduced tumor spheroid area starting from the dose of 1 μM for both cell types (Fig. 2E and 2F). Moreover, Fingolimod significantly enhanced cell apoptosis and death starting from the dose of 10 μM for both cell lines and significantly promoted cytotoxicity already after one day of treatment for BT20 (Fig. 2G and 2H).

Altogether, these data suggest that Cisplatin reduces tumor growth at doses devoid of effect on cell apoptosis or death in 3D tumor spheroid models. Conversely, Fingolimod is able to reduce tumor growth in a manner which is related to an increase of cell apoptosis and death.

Fingolimod decreased TNBC tumor growth in vivo in orthotopic immunocompetent and immunodeficient mouse models

A syngeneic mouse metastatic breast cancer model, in which 4T1 murine TNBC cells were implanted into the mammary fat pad of immunocompetent mice, was used to examine the potential effect of drugs on TNBC progression in vivo. The mice were treated with Fingolimod or Cisplatin either as monotherapy or in combination. Mice treated with monotherapies or combination therapy showed a significant decrease in tumor volume when compared to vehicle treated animals (Fig. 3A). Interestingly, the repression of tumor growth was significantly higher in Fingolimod-treated mice compared to Cisplatin (Fig. 3A). A combination of treatments significantly improved the anti-tumor effect compared with Cisplatin, but not with Fingolimod, suggesting no synergistic effect of treatments (Fig. 3A). Analysis of tumor weight after sacrifice confirmed the significant anti-tumor effect of Fingolimod and combination therapy (Fig. 3B). Cisplatin did not significantly reduce tumor weight, while Fingolimod and the combination had a higher inhibitory effect compared to Cisplatin, significantly so for the combination (Fig. 3B). These data suggest a higher anti-tumor effect of Fingolimod compared to Cisplatin on primary tumors in the 4T1 orthotopic TNBC model.

The 4T1 tumor model presents distant metastases in different organs including lungs, liver, and spleen [42,43]. We analyzed the effect of treatments on macro-metastasis formation in lungs, liver, and spleen after necropsy. We did not observe any differences regarding visible lung macro-lesions or lung weight, suggesting an absence of effect of both drugs on lung metastasis formation (Fig. 3C–D). Conversely, we identified that all treatments tended to reduce liver macro-lesions and significantly decreased liver weight and spleen macro-lesions compared to the control (Fig. 3E–G). Moreover, the combination of treatments demonstrated significantly higher spleen macro-metastasis reduction compared to Fingolimod alone (Fig. 3G). These data suggest that Cisplatin and Fingolimod displayed liver and spleen anti-metastatic effects while they did not affect lung metastases. Fingolimod did not demonstrate better anti-metastatic effects than Cisplatin.

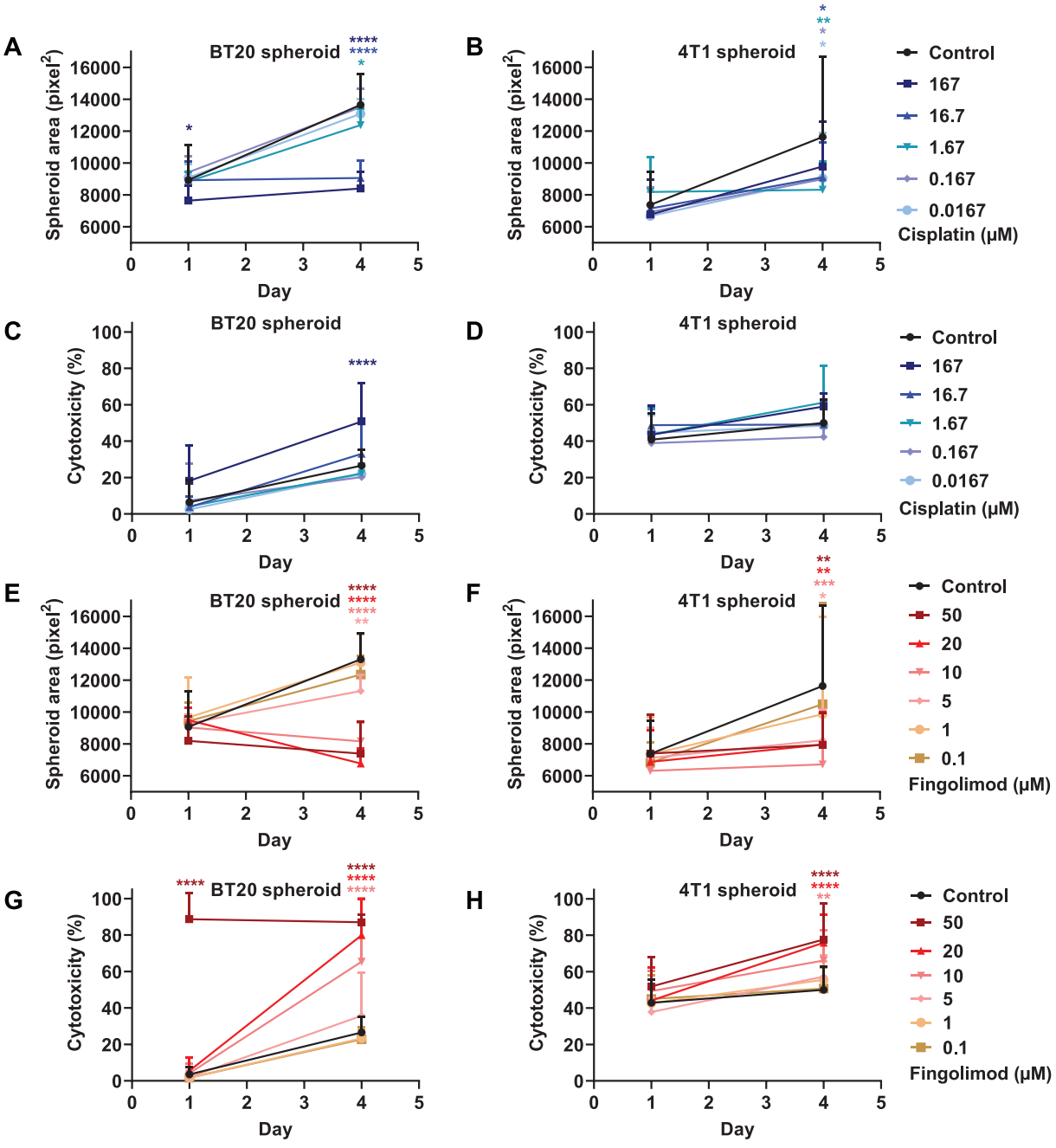

Fig. 2. Effects of Cisplatin and Fingolimod on TNBC in 3D tumor spheroid assay.
A-H. Dose-response effect of Cisplatin (A-D) and Fingolimod (E-H) treatment on 4T1 and BT20 using 3D tumor spheroid assay.
The study was done with seven to eight replicates from two independent experiments. Data represent mean and SD. Statistical differences between the groups were determined using two-way ANOVA (groups and time as factor) followed by Bonferroni's multiple comparisons test (vs. control, * $p \leq 0.05$, ** $p \leq 0.01$, *** $p \leq 0.001$, **** $p \leq 0.0001$).

The effect of Fingolimod as a monotherapy on tumor growth and weight was confirmed in another study with a smaller cohort (Fig. S5A-B). Fingolimod did not affect mouse survival (Fig. S5C) or lung weight, used as an indicator of tumor metastasis (Fig. S5D).

In order to further evaluate the role of Fingolimod in TNBC, we also challenged Fingolimod and Cisplatin as monotherapy in another mouse xenograft model. We used reporter human MDA-MB-231-RFP-Luc cells xenografted in immunodeficient mice. Bioluminescence monitoring of tumor growth and RFP was used for ex vivo analysis of metastasis formation. Mice treated with Fingolimod or Cisplatin displayed significant reduced bioluminescence signals (Fig. 4A–B) consistently with reduced tumor volume (Fig. 4C). We did not observe a significant higher anti-tumor effect of Fingolimod in comparison to Cisplatin, in contrast with the syngeneic model (Fig. 3A). In addition, we analyzed the effect of treatments on macro-metastasis formation in lungs using fluorescence imaging, but we did not observe a reduction of lung metastasis burden (Fig. 4D–E). No liver or spleen macro-metastases were observed in this model. We confirmed this observation in a purely metastasis model in which MDA-MB-231-RFP-Luc cells were injected into mice's tail vein (i.v.). In this model, cancer cells travel directly to the lung rather than

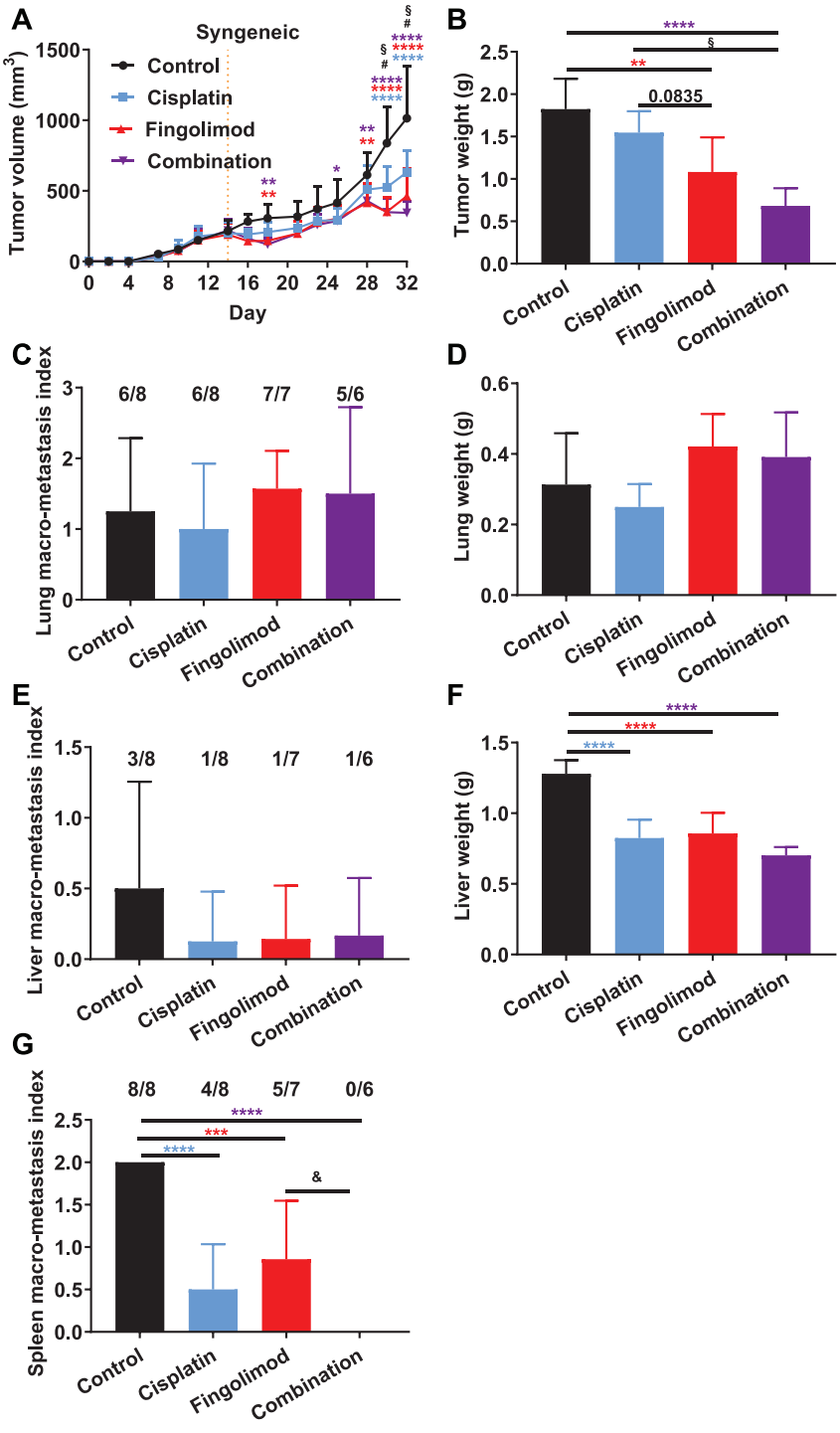

Fig. 3. Effects of Fingolimod and Cisplatin in a syngeneic orthotopic TNBC mouse model.

A-B. Impact of Cisplatin and Fingolimod treatment on 4T1 mouse TNBC in vivo tumor volume (A) and ex vivo tumor weight (B). Discontinuous orange line highlights treatment beginning. C-G. Macroscopic analysis of in vivo macro-metastasis index onto both lungs (C), liver (E), and spleen (G) and ex vivo quantification of lung (D) and liver (F) weight. Fractions above the bars indicate the number of organs with visible metastasis.

Discontinuous orange line highlights treatment beginning. Cisplatin was administered at 1 mg/kg and Fingolimod at 5 mg/kg, i.p. 5 times per week for both grafting models. Two-way using mixed-effects model (REML) (A, B) or one-way (C-G) ANOVA test followed by Tukey's multiple comparisons test (vs. control, * $p \leq 0.05$, ** $p \leq 0.01$, *** $p \leq 0.001$, **** $p \leq 0.0001$; Cisplatin vs. Fingolimod, # $p \leq 0.05$; Cisplatin vs. Combination, § $p \leq 0.05$; Fingolimod vs. Combination, & $p \leq 0.05$). Data represent mean and SD. $n = 8$ mice per group at the start of treatment.

escaping from a primary tumor [44]. Metastasis progression in this i.v. model, using bioluminescence imaging, was not affected by Cisplatin or Fingolimod (Fig. S6).

Fingolimod decreased TNBC tumor recurrence after primary tumor resection in a translational immunocompetent mouse model

Tumor surgical resection upon diagnosis is the standard of care for breast cancer [45]. In order to mimic the clinical practice, we developed a tumor resection model based on the syngeneic orthotopic TNBC model using 4T1 cells. After surgical resection of the tumor, mice were monitored and tumor regrowth was analyzed upon treatment (Fig. 5A). Mice treated with Fingolimod or Cisplatin exhibited significant reduction of tumor recurrence with lower tumor volume regrowth compared to the control group (Fig. 5B).

Fingolimod is well tolerated in vivo

We also investigated the effect of treatments on mouse body weight and mouse behavior according to the parameters defined as ethical limits. Fingolimod did not affect mouse body weight compared to control in our two experimental studies with the syngeneic model using 4T1 cells (Figs. 6A and S6) or with the xenograft model using MDA-MB-231-RFP-Luc labeled cells (Fig. 6B). Conversely, Cisplatin significantly decreased

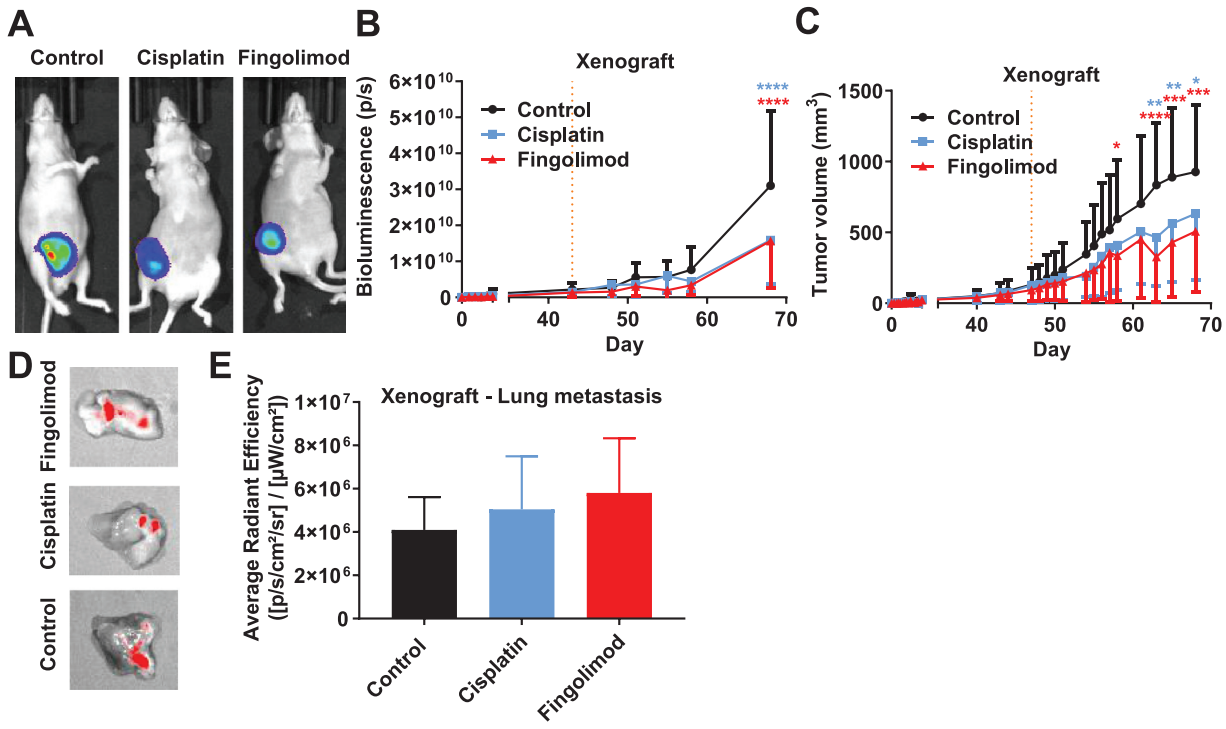

Fig. 4. Effects of Fingolimod and Cisplatin in an orthotopic xenograft TNBC mouse model.
A-B Impact of Cisplatin and Fingolimod treatment on MDA-MB-231-RFP-Luc human TNBC xenograft tumor growth using in vivo bioluminescence imaging. Representative pictures (A) and quantification by bioluminescence signal (B). Bioluminescence images are obtained by injecting i.p. luciferin at 150 mg/kg 10 min before image acquisition. C. Impact of Cisplatin and Fingolimod treatment on MDA-MB-231-RFP-Luc human TNBC xenograft tumor volume measured using caliper. D-E. Impact of Cisplatin and Fingolimod treatment on MDA-MB-231-RFP-Luc human TNBC xenograft metastasis formation. Representative pictures of fluorescent signal expressed by tumor cells in mouse lungs (D) and quantification through red fluorescent protein (RFP) signal detection ex vivo (E).
Discontinuous orange line highlights treatment beginning. Cisplatin was administered at 1 mg/kg and Fingolimod at 5 mg/kg, i.p. 5 times per week. Two-way (B, C) and one-way (E) ANOVA test followed by Bonferroni's multiple comparisons test (versus control, * $p \leq 0.05$, ** $p \leq 0.01$, *** $p \leq 0.001$, **** $p \leq 0.0001$). Data represent mean and SD. $n = 6$ mice per group at the start of treatment.

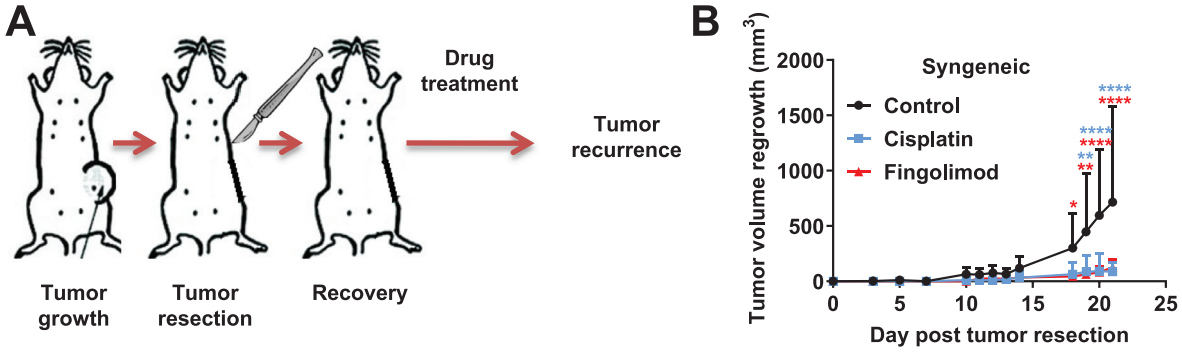

Fig. 5. Effects of Cisplatin and Fingolimod on tumor recurrence after primary breast tumor resection.
A. Procedure for the breast cancer resection model and associated tumor relapse and survival analysis. B. Analysis of Cisplatin and Fingolimod anti-tumor activity post primary tumor resection in the 4T1 mouse TNBC syngeneic grafting model. Quantification of the tumor volume by caliper.
Cisplatin at 1 mg/kg or Fingolimod at 5 mg/kg treatment i.p. 5 times a week starting two days after tumor resection (day 2). Two-way ANOVA test followed by Bonferroni's multiple comparisons test (vs. control, * $p \leq 0.05$, ** $p \leq 0.01$, **** $p \leq 0.0001$). Survival curves were constructed using the Kaplan-Meier method and analyzed by log rank test. Data represent mean and SD. $n = 6$ mice per group at the start of treatment.

mouse body weight over time in both syngeneic and xenograft models (Fig. 6A-B). The combination of treatments significantly decreased mouse body weight compared to the control and Fingolimod-treated groups. No significant difference was observed between Cisplatin and the combination, suggesting that toxicity may be due to Cisplatin alone (Fig. 6A). In contrast to Cisplatin, no obvious effect on mouse behavior was observed in groups treated with Fingolimod during the studies. Altogether, these data suggest that Fingolimod was well tolerated in mice.

Discussion

Data from the literature suggests that the S1P protein level is elevated in breast cancer tissue [9] and that tumor invasion into lymph nodes is associated with higher levels of S1P in breast cancer [46]. S1P targeting therefore seems to be a relevant strategy to limit TNBC progression [14]. In this work, we used Fingolimod as a pharmacological tool, described in the literature to target S1P axis [14], in TNBC in vitro and in vivo models, and demonstrated preclinical efficacy of Fingolimod

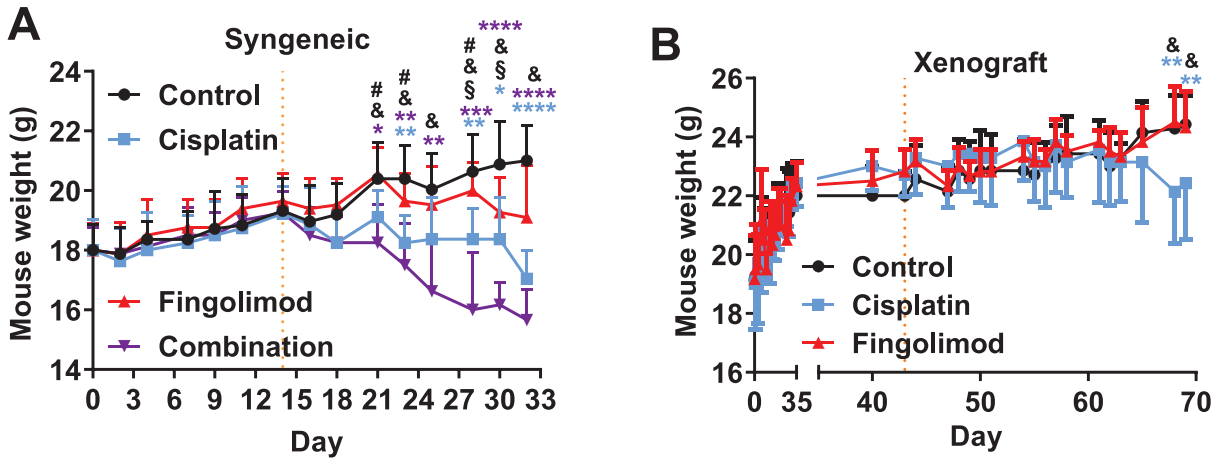

Fig. 6. Effects of Cisplatin and Fingolimod on tumor-bearing mouse body weight.
A-B. Measure and comparison of mouse body weight upon Cisplatin at 1 mg/kg or Fingolimod at 5 mg/kg treatment i.p. 5 times per week in the 4T1 syngeneic breast cancer model (A) and in the MDA-MB-231-RFP-Luc xenograft breast cancer model (B). Discontinuous orange line highlights treatment beginning.
Two-way ANOVA test (Mixed-effects model) followed by Tukey's multiple comparisons test (vs. control * $p \leq 0.05$, ** $p \leq 0.01$, **** $p \leq 0.0001$; Cisplatin vs. Fingolimod, # $p \leq 0.05$; Cisplatin vs. Combination, § $p \leq 0.05$; Fingolimod vs. Combination, & $p \leq 0.05$). Data represent mean and SD. $n = 8$ (A) and 6 (B) mice per group at the start of treatment.

for reducing tumor progression. We trust that these encouraging data will stimulate further preclinical studies evaluating the mechanism of action of Fingolimod.

Fingolimod was developed as an immunosuppressive drug for the treatment of multiple sclerosis. Fingolimod induces the retention of lymphocytes in secondary lymphoid organs thereby reducing peripheral circulating lymphocytes. Fingolimod also displays anti-cancer efficacy in animal models of cancer [13,14]. However, the mechanisms of action of Fingolimod are diverse and have yet to be fully characterized. The use of in vitro cell viability and in vivo tumor graft models in immunocompetent or immunodeficient mice (lacking functional T cells), showed that Fingolimod represses primary tumor progression and metastasis formation. A similar anti-tumor response was observed in immunocompetent and immunodeficient mice, suggesting a T cell independent response. Moreover, we demonstrated that Fingolimod is able to directly affect TNBC cell survival in vitro. Several research teams demonstrated similar anti-proliferative effects of Fingolimod in multiple cancer cell lines including hepatocellular carcinoma, prostate cancer, and ovarian cancer cells [16,17,47,48]. We also observed that Fingolimod induces tumor cell death in 2D and 3D in vitro models, consistent with described data in other tumor indications such as hepatoma [49]. Our data indicated that Fingolimod reduces tumor growth through an increase of cancer cell apoptosis and death (Fig. 2). In contrast, Fingolimod has minimal effects on normal cells [13], suggesting an interest for its repurposing as an anti-cancer drug for TNBC. Cisplatin, on the other hand, reduces tumor growth in 3D tumor spheroid models with less effect on cell apoptosis and death, except at high dose. The effect of Cisplatin is likely a result of inhibition of replication by Cisplatin-DNA adducts rather than a stimulation of apoptosis signaling, such as caspase- or p73-derived pathways [50,51].

Fingolimod interferes with several mechanisms and related pathways affecting tumor mobility [13,14]. We demonstrated that Fingolimod reduces liver and spleen macro-metastasis formation in 4T1 orthotopic syngeneic models. In contrast, we did not observe any effect of Fingolimod on lung macro-metastasis formation in either 4T1 or MDA-MB-231-RFP-Luc orthotopic graft models and also in experimental metastasis model with MDA-MB-231-RFP-Luc cells, suggesting differential Fingolimod-related mechanism of action between lung, liver or spleen. Fingolimod has already been shown to repress in vitro migration and invasion capacities of prostate [22] or medulloblastoma cells [52]. Fingolimod inhibits of RhoA/Rac/ROCK-1 signaling in macrophage [53], and RhoA and in prostate cancer and glioblastoma cells, leading to reduced tumor cell mobility and invasion [43,54]. Fingolimod also downregulates markers of epithelial-to-mesenchymal transition (EMT) in tumor cells [55,56], suggesting its possible efficacy against tumor cell migration and invasion. In vivo, Fingolimod limits lung metastases in the hepatocellular carcinoma xenograft model [57,58] and in the melanoma syngeneic model [59], however, Fingolimod did not affect the number of distant metastases (lungs, liver, pancreas, mesenteric and kidney) in a prostate xenograft model [17], suggesting cancer type-related response. In breast cancer, Fingolimod suppresses lung metastases in high fat diet models of transgenic and syngeneic orthotopic TNBC mice, when administrated in prophylaxis before tumor cell injection [25] whereas it did not affect lung metastases in a normal diet syngeneic orthotopic model when treatment started after tumor cell injection [60]. In the present study, we evaluated the effect of Fingolimod on lung metastases in a syngeneic model of TNBC and, to our knowledge, for the first time in a xenograft model. We did not observe an effect of Fingolimod on lung metastases in both models (Figs. 2, 3, and S6). This observation, at least in the 4T1 syngeneic orthotopic model, is consistent with the data from Spitzer and collaborators [60], but opposite to those described by Nagahashi et al. [34]. Nevertheless, in our work, as with Spitzer et al., mice were treated after metastasis apparition. These data suggest that Fingolimod might not serve interventional therapy to target lung metastases. Conversely, and to our knowledge, we have demonstrated for the first time, in the syngeneic TNBC mouse model, that Fingolimod is able to repress liver and spleen distant metastases. Breast cancer-derived spleen metastases are rare in patients but represent classical metastases sites for murine model [61–63]. Conversely, liver metastases represent a common site of metastases in breast cancer and is correlated with poor survival in patient with higher risk to patient death as compared to lung metastases [63,64]. Thus, Fingolimod might provide valuable clinical advantage for treating in particular liver metastases. Preferred organotropism for breast cancer distant metastatic site is currently investigated and is influenced multiple factors including genetic alterations and protein expression. As an example, signaling pathway such a $\alpha v \beta 5$ integrin expression by tumor cells favors liver metastases whereas $\alpha 6 \beta 1$ seems to favor lung metastases [63]. Interestingly, CXCR4/CXCL12 signaling has been described to be particularly involved in liver extravasation of tumor cells within the liver [63]. Remarkably, Fingolimod has

been already described to modulate CXCR4/CXCL12 axis in experimental models of multiple myeloma, prostate cancer, and multiple sclerosis [65–67], and might therefore more specifically affect liver and not lung metastases. Fingolimod is also described to affect the morphology of the tumor through modification of the vascular architecture by promoting tissue remodeling, vessel normalization, and reduced hypoxia [18], all important mechanisms participating to tumor relapse [2]. In patients with multiple sclerosis, Fingolimod represses T cell mobilization from lymphoid tissues, which generally results in leucopenia [11]. This adverse effect of Fingolimod might be deleterious for breast cancer patients. Nevertheless, low lymphocyte count is not necessarily associated with poor prognosis [68,69]. Moreover, Spranger and collaborators demonstrated in a syngeneic melanoma model using B16F10 cells that concomitant administration of Fingolimod with an immune checkpoint inhibitor did not affect their efficacy and even enhanced their anti-tumoral effect. They also observed that despite a reduction of CD3 positive cells in peripheral blood, T cell infiltration within the tumor tissue was not affected [70], suggesting that immune-related effects in the tumor microenvironment are not involved in Fingolimod-derived tumor response. Martin and collaborators observed a poor therapeutic effect of Fingolimod on 4T1 tumor growth in immunodeficient mice lacking T cells. Conversely when injected in immunocompetent mice, Fingolimod induced an anti-tumoral effect [27], suggesting a potential role of T cells in Fingolimod response. Conversely, in our assay we observed an anti-tumoral response of Fingolimod with MDA-MB-231-RFP-Luc cells xenografted in immunodeficient mice lacking functional T cells. In addition, previous work showed that Fingolimod is not associated with a change in CD3 positive cell infiltration into the tumor tissue in immunocompetent rat liver tumor model [49], suggesting an absence of effect of Fingolimod on the T cell response in the tumor microenvironment. Several research teams also described anti-tumoral effects of Fingolimod in a xenograft model lacking functional T cells [13,14]. Altogether, these data tend to suggest complex and model-dependent anti-tumoral effects of Fingolimod.

To our knowledge, no clinical study investigated the efficacy of Fingolimod in cancer, only one safety study (NCT02490930) is currently completed for patients with glioma in which Fingolimod is associated with radiation and Temozolomide. Nevertheless, no results have currently been published and the dose of Fingolimod used in this study is based on the posology used for multiple sclerosis of 0.5 mg per day. At this dose, basal blood concentration of Fingolimod for patients with multiple sclerosis could vary between 10 and 100 ng/mL [71,72] Snelder et al. showed that higher doses of Fingolimod increased blood concentration in human [71], with good safety profile for chronic doses for up to 5 mg per day [73] and for single dose for up to 40 mg [74]. Our in vitro assay showed that the anti-cancer effect of Fingolimod is observed with doses starting from 5 µM (Fig. 2) which is equivalent of around 1 µg/mL. This anti-cancer effect is also observed at similar dosing in other tumor preclinical models [17,75]. Therefore, a higher dose of Fingolimod starting from 10 mg/day might represent an interesting clinical dosing for patients with cancer, suggesting that further clinical and safety investigations might be particularly useful.

The therapeutic benefit of Cisplatin in breast cancer treatments is often limited due to resistance [76]. We identified that Cisplatin reduced tumor growth without affecting lung metastasis formation in our TNBC mouse models, consistent with similar observations on primary tumor growth [28,31,37,38,77,78]. We showed that Fingolimod has a similar efficacy as Cisplatin without associated chemotherapy-related toxicity. Indeed, Fingolimod was well tolerated in vivo, as indicated by the absence of effect on mouse body weight or behavior in our experimental models. Additional measurements, such as histopathological analysis, would complement this data, in order to exclude in vivo toxicity. In patients with multiple sclerosis, Fingolimod demonstrated a very good safety profile with manageable adverse events [79]. Regarding this aspect, and in comparison with adverse effects of chemotherapeutic agents such as Cisplatin, Fingolimod might represent an interesting avenue as an anti-cancer agent in patients with TNBC.

In our study, we do not observe a synergistic effect of Fingolimod and the chemotherapeutic agent, Cisplatin, in the mouse 4T1 TNBC orthotopic model (Fig. 3). Fingolimod alone demonstrates higher or similar therapeutic efficacy compared to Cisplatin alone in our different models. Conversely, Fingolimod potentiates the anti-cancer effects of Carboplatin in ovarian and breast cancer model [47,80] and radiation-based therapy in prostate cancer [17]. Cisplatin and Fingolimod are described to have similar modes of action on common signaling pathways. Both drugs, for example, modulate MAPK or AKT-related downstream signaling [13,14,37,51,76]. An effect on common pathways may therefore explain the poor or lack of synergy between Cisplatin and Fingolimod observed in the timeframe of our in vivo experiments. This suggests that Fingolimod might be used as a substitute rather than in combination to platinum-based molecule for TNBC.

In conclusion, we have confirmed an anti-cancer effect of Fingolimod on primary tumor, and liver and spleen metastases, in TNBC orthotopic mouse models, not associated with obvious safety concerns. This work provides a preclinical proof of concept of the therapeutic value of Fingolimod for the breast cancer tumor research community, and more specifically for TNBC.

Declaration of Competing Interest

The authors are all employees of Porsolt and declare no conflict of interest.

CRediT authorship contribution statement

Tristan Rupp: Conceptualization, Methodology, Formal analysis, Writing - original draft , Writing - review & editing, Visualization, Supervision. **Océane Pelouin:** Investigation, Validation. **Laurie Genest:** Investigation, Validation. **Christophe Legrand:** Investigation. **Guillaume Froget:** Supervision. **Vincent Castagné:** Methodology, Writing - review & editing.

Acknowledgments

We thank David Pushett for reading the manuscript and providing helpful comments regarding English. We thank Claire Duquesnoy for illustrating the graphical abstract.

Funding

The work was fully supported by Porsolt SAS.

Supplementary materials

Supplementary material associated with this article can be found, in the online version, at doi:10.1016/j.tranon.2020.100926.

References

[1] F. Cardoso, E. Senkus, A. Costa, E. Papadopoulos, M. Aapro, F. André, et al., 4th ESO-ESMO international consensus guidelines for advanced breast cancer (ABC 4)†, Ann. Oncol. 29 (2018) 1634–1657, doi:10.1093/annonc/mdy192.
[2] N. Harbeck, F. Penault-Llorca, J. Cortes, M. Gnant, N. Houssami, P. Poortmans, et al., Breast cancer, Nat. Rev. Dis. Primers 5 (2019) 1–31, doi:10.1038/s41572-019-0111-2.
[3] R. Dent, M. Trudeau, K.I. Pritchard, W.M. Hanna, H.K. Kahn, C.A. Sawka, et al., Triple-negative breast cancer: clinical features and patterns of recurrence, Clin. Cancer Res. 13 (2007) 4429–4434, doi:10.1158/1078-0432.CCR-06-3045.
[4] M. Nagahashi, M. Abe, K. Sakimura, K. Takabe, T. Wakai, The role of sphingosine-1-phosphate in inflammation and cancer progression, Cancer Sci. 109 (2018) 3671–3678, doi:10.1111/cas.13802.
[5] N.J. Pyne, S. Pyne, Sphingosine 1-phosphate and cancer, Nat. Rev. Cancer 10 (2010) 489–503, doi:10.1038/nrc2875.

[6] G. Grammatikos, N. Schoell, N. Ferreirós, D. Bon, E. Herrmann, H. Farnik, et al., Serum sphingolipidomic analyses reveal an upregulation of C16- ceramide and sphingosine-1-phosphate in hepatocellular carcinoma, Oncotarget 7 (2016) 18095–18105, doi:10.18632/oncotarget.7741.

[7] Y. Zeng, X. Yao, L. Chen, Z. Yan, J. Liu, Y. Zhang, et al., Sphingosine-1-phosphate induced epithelial-mesenchymal transition of hepatocellular carcinoma via an MMP-7/syndecan-1/TGF-β autocrine loop, Oncotarget 7 (2016) 63324–63337, doi:10.18632/oncotarget.11450.

[8] Y. Hirose, M. Nagahashi, E. Katsuta, K. Yuza, K. Miura, J. Sakata, et al., Generation of sphingosine-1-phosphate is enhanced in biliary tract cancer patients and is associated with lymphatic metastasis, Sci. Rep. 8 (2018), doi:10.1038/s41598-018-29144-9.

[9] M. Nagahashi, J. Tsuchida, K. Moro, M. Hasegawa, K. Tatsuda, I.A. Woelfel, et al., High levels of sphingolipids in human breast cancer, J. Surg. Res. 204 (2016) 435–444, doi:10.1016/j.jss.2016.05.022.

[10] S. Wang, Y. Liang, W. Chang, B. Hu, Y. Zhang, Triple negative breast cancer depends on sphingosine kinase 1 (SphK1)/sphingosine-1-phosphate (S1P)/sphingosine 1-phosphate receptor 3 (S1PR3)/notch signaling for metastasis, Med. Sci. Monit. 24 (2018) 1912–1923, doi:10.12659/MSM.905833.

[11] M. Tintore, A. Vidal-Jordana, J. Sastre-Garriga, Treatment of multiple sclerosis — success from bench to bedside, Nat. Rev. Neurol. 15 (2019) 53–58, doi:10.1038/s41582-018-0082-z.

[12] K. Geffken, S. Spiegel, Sphingosine kinase 1 in breast cancer, Adv. Biol. Regul. 67 (2018) 59–65, doi:10.1016/j.jbior.2017.10.005.

[13] S.N. Patmanathan, L.F. Yap, P.G. Murray, I.C. Paterson, The antineoplastic properties of FTY720: evidence for the repurposing of Fingolimod, J. Cell. Mol. Med. 19 (2015) 2329–2340, doi:10.1111/jcmm.12635.

[14] C. White, H. Alshaker, C. Cooper, M. Winkler, D. Pchejetski, The emerging role of FTY720 (Fingolimod) in cancer treatment, Oncotarget 7 (2016) 23106–23127, doi:10.18632/oncotarget.7145.

[15] R. Rosa, R. Marciano, U. Malapelle, L. Formisano, L. Nappi, C. D'Amato, et al., Sphingosine kinase 1 overexpression contributes to cetuximab resistance in human colorectal cancer models, Clin. Cancer Res. 19 (2013) 138–147, doi:10.1158/1078-0432.CCR-12-1050.

[16] J.W.Y. Ho, K. Man, C.K. Sun, T.K. Lee, R.T.P. Poon, S.T. Fan, Effects of a novel immunomodulating agent, FTY720, on tumor growth and angiogenesis in hepatocellular carcinoma, Mol. Cancer Ther. 4 (2005) 1430–1438, doi:10.1158/1535-7163.MCT-05-0021.

[17] D. Pchejetski, T. Bohler, L. Brizuela, L. Sauer, N. Doumerc, M. Golzio, et al., FTY720 (Fingolimod) sensitizes prostate cancer cells to radiotherapy by inhibition of sphingosine kinase-1, Cancer Res. 70 (2010) 8651–8661, doi:10.1158/0008-5472.CAN-10-1388.

[18] C. Gstalder, I. Ader, O. Cuvillier, FTY720 (Fingolimod) inhibits HIF1 and HIF2 signaling, promotes vascular remodeling, and chemosensitizes in renal cell carcinoma animal model, Mol. Cancer Ther. 15 (2016) 2465–2474, doi:10.1158/1535-7163.MCT-16-0167.

[19] K. LaMontagne, A. Littlewood-Evans, C. Schnell, T. O'Reilly, L. Wyder, T. Sanchez, et al., Antagonism of sphingosine-1-phosphate receptors by FTY720 inhibits angiogenesis and tumor vascularization, Cancer Res. 66 (2006) 221–231, doi:10.1158/0008-5472.CAN-05-2001.

[20] B. Langlois, F. Saupe, T. Rupp, C. Arnold, M. van der Heyden, G. Orend, et al., AngioMatrix, a signature of the tumor angiogenic switch-specific matrisome, correlates with poor prognosis for glioma and colorectal cancer patients, Oncotarget 5 (2014) 10529–10545, doi:10.18632/oncotarget.2470.

[21] T. Rupp, B. Langlois, M.M. Koczorowska, A. Radwanska, Z. Sun, T. Hussenet, et al., Tenascin-C orchestrates glioblastoma angiogenesis by modulation of pro- and anti-angiogenic signaling, Cell Rep. 17 (2016) 2607–2619, doi:10.1016/j.celrep.2016.11.012.

[22] V. Kalhori, M. Magnusson, M.Y. Asghar, I. Pulli, K. Törnquist, FTY720 (Fingolimod) attenuates basal and sphingosine-1-phosphate-evoked thyroid cancer cell invasion, Endocr. Relat. Cancer 23 (2016) 457–468, doi:10.1530/ERC-16-0050.

[23] H. Azuma, S. Takahara, N. Ichimaru, J.D. Wang, Y. Itoh, Y. Otsuki, et al., Marked prevention of tumor growth and metastasis by a novel immunosuppressive agent, FTY720, in mouse breast cancer models, Cancer Res. 62 (2002) 1410–1419.

[24] Y. Mousseau, S. Mollard, K. Faucher-Durand, L. Richard, A. Nizou, J. Cook-Moreau, et al., Fingolimod potentiates the effects of sunitinib malate in a rat breast cancer model, Breast Cancer Res. Treat. 134 (2012) 31–40, doi:10.1007/s10549-011-1903-6.

[25] M. Nagahashi, A. Yamada, E. Katsuta, T. Aoyagi, W.-.C. Huang, K.P. Terracina, et al., Targeting the SphK1/S1P/S1PR1 axis that links obesity, chronic inflammation, and breast cancer metastasis, Cancer Res. 78 (2018) 1713–1725, doi:10.1158/0008-5472.CAN-17-1423.

[26] X. Dai, H. Cheng, Z. Bai, J. Li, Breast cancer cell line classification and its relevance with breast tumor subtyping, J. Cancer 8 (2017) 3131–3141, doi:10.7150/jca.18457.

[27] J.L. Martin, S.M. Julovi, M.Z. Lin, H.C. de Silva, F.M. Boyle, R.C. Baxter, Inhibition of basal-like breast cancer growth by FTY720 in combination with epidermal growth factor receptor kinase blockade, Breast Cancer Res. (2017) 19, doi:10.1186/s13058-017-0882-x.

[28] S. Liang, X. Peng, X. Li, P. Yang, L. Xie, Y. Li, et al., Silencing of CXCR4 sensitizes triple-negative breast cancer cells to cisplatin, Oncotarget 6 (2014) 1020–1030.

[29] L.R. Gomes, C.R.R. Rocha, D.J. Martins, A.P.Z.P. Fiore, G.S. Kinker, A. Bruni-Cardoso, et al., ATR mediates cisplatin resistance in 3D-cultured breast cancer cells via translesion DNA synthesis modulation, Cell Death. Dis. 10 (2019) 1–15, doi:10.1038/s41419-019-1689-8.

[30] G. Marvaso, A. Barone, N. Amodio, L. Raimondi, V. Agosti, E. Altomare, et al., Sphingosine analog fingolimod (FTY720) increases radiation sensitivity of human breast cancer cells in vitro, Cancer Biol. Ther. 15 (2014) 797–805, doi:10.4161/cbt.28556.

[31] Y. Chen, F. Han, L. Cao, C. Li, J. Wang, Q. Li, et al., Dose-response relationship in cisplatin-treated breast cancer xenografts monitored with dynamic contrast-enhanced ultrasound, BMC Cancer 15 (2015), doi:10.1186/s12885-015-1170-8.

[32] Z. Liang, Y. Yoon, J. Votaw, M.M. Goodman, L. Williams, H. Shim, Silencing of CXCR4 Blocks Breast Cancer Metastasis, Cancer Res. 65 (2005) 967–971.

[33] S.M. Woo, B.R. Seo, K. Min, T.K. Kwon, FTY720 enhances TRAIL-mediated apoptosis by up-regulating DR5 and down-regulating Mcl-1 in cancer cells, Oncotarget 6 (2015) 11614–11626.

[34] M. Nagahashi, S. Ramachandran, E.Y. Kim, J.C. Allegood, O.M. Rashid, A. Yamada, et al., Sphingosine-1-phosphate produced by sphingosine kinase 1 promotes breast cancer progression by stimulating angiogenesis and lymphangiogenesis, Cancer Res. 72 (2012) 726–735, doi:10.1158/0008-5472.CAN-11-2167.

[35] D.P. Hill, A. Harper, J. Malcolm, M.S. McAndrews, S.M. Mockus, S.E. Patterson, et al., Cisplatin-resistant triple-negative breast cancer subtypes: multiple mechanisms of resistance, BMC Cancer 19 (2019) 1039, doi:10.1186/s12885-019-6278-9.

[36] X.-.C. Hu, J. Zhang, B.-.H. Xu, L. Cai, J. Ragaz, Z.-.H. Wang, et al., Cisplatin plus gemcitabine versus paclitaxel plus gemcitabine as first-line therapy for metastatic triple-negative breast cancer (CBCSG006): a randomised, open-label, multicentre, phase 3 trial, Lancet Oncol. 16 (2015) 436–446, doi:10.1016/S1470-2045.

[37] J. Park, T.S. Morley, P.E. Scherer, Inhibition of endotrophin, a cleavage product of collagen VI, confers cisplatin sensitivity to tumours, EMBO Mol. Med. 5 (2013) 935–948, doi:10.1002/emmm.201202006.

[38] H. Yu, C. Guo, B. Feng, J. Liu, X. Chen, D. Wang, et al., Triple-layered pH-responsive micelleplexes loaded with siRNA and cisplatin prodrug for NF-Kappa B targeted treatment of metastatic breast cancer, Theranostics 6 (2016) 14–27, doi:10.7150/thno.13515.

[39] M. Zanoni, F. Piccinini, C. Arienti, A. Zamagni, S. Santi, R. Polico, et al., 3D tumor spheroid models for in vitro therapeutic screening: a systematic approach to enhance the biological relevance of data obtained, Sci. Rep. 6 (2016) 19103, doi:10.1038/srep19103.

[40] Y.T. Phung, D. Barbone, V.C. Broaddus, M. Ho, Rapid generation of in vitro multicellular spheroids for the study of monoclonal antibody therapy, J. Cancer 2 (2011) 507–514.

[41] S. Sant, P.A. Johnston, The production of 3D tumor spheroids for cancer drug discovery, Drug Discov. Today Technol. 23 (2017) 27–36, doi:10.1016/j.ddtec.2017.03.002.

[42] S. Swami, J. Johnson, L.A. Bettinson, T. Kimura, H. Zhu, M.A. Albertelli, et al., Prevention of breast cancer skeletal metastases with parathyroid hormone, JCI Insight 2 (2017), doi:10.1172/jci.insight.90874.

[43] Y. Zhang, N. Zhang, R.M. Hoffman, M. Zhao, Surgically-induced multi-organ metastasis in an orthotopic syngeneic imageable model of 4T1 murine breast cancer, Anticancer Res. 35 (2015) 4641–4646.

[44] M.R. Cominetti, W.F. Altei, H.S. Selistre-de-Araujo, Metastasis inhibition in breast cancer by targeting cancer cell extravasation, Breast Cancer (Dove Med Press) 11 (2019) 165–178, doi:10.2147/BCTT.S166725.

[45] M. Lambertini, F. Poggio, M. Bruzzone, B. Conte, C. Bighin, E. de Azambuja, et al., Dose-dense adjuvant chemotherapy in HER2-positive early breast cancer patients before and after the introduction of trastuzumab: exploratory analysis of the GIM2 trial, Int. J. Cancer (2019), doi:10.1002/ijc.32789.

[46] J. Tsuchida, M. Nagahashi, M. Nakajima, K. Moro, K. Tatsuda, R. Ramanathan, et al., Breast cancer S1P is associated with pSphK1 and lymphatic metastasis, J. Surg. Res. 205 (2016) 85–94, doi:10.1016/j.jss.2016.06.022.

[47] K.M. Kreitzburg, S.C. Fehling, C.N. Landen, T.L. Gamblin, R.B. Vance, R.C. Arend, et al., FTY720 enhances the anti-tumor activity of carboplatin and tamoxifen in a patient-derived xenograft model of ovarian cancer, Cancer Lett. 436 (2018) 75–86, doi:10.1016/j.canlet.2018.08.015.

[48] L.L. Stafman, A.P. Williams, R. Marayati, J.M. Aye, J.E. Stewart, E. Mroczek-Musulman, et al., PP2A activation alone and in combination with cisplatin decreases cell growth and tumor formation in human HuH6 hepatoblastoma cells, PLoS One 14 (2019), doi:10.1371/journal.pone.0214469.

[49] K.T. Ng, K. Man, J.W. Ho, C.K. Sun, T.K. Lee, Y. Zhao, et al., Marked suppression of tumor growth by FTY720 in a rat liver tumor model: the significance of down-regulation of cell survival Akt pathway, Int. J. Oncol. 30 (2007) 375–380, doi:10.3892/ijo.30.2.375.

[50] Z.H. Siddik, Cisplatin: mode of cytotoxic action and molecular basis of resistance, Oncogene 22 (2003) 7265–7279, doi:10.1038/sj.onc.1206933.

[51] S. Dasari, P.B. Tchounwou, Cisplatin in cancer therapy: molecular mechanisms of action, Eur. J. Pharmacol. 0 (2014) 364–378, doi:10.1016/j.ejphar.2014.07.025.

[52] E.F. Garner, A.P. Williams, L.L. Stafman, J.M. Aye, E. Mroczek-Musulman, B.P. Moore, et al., FTY720 decreases tumorigenesis in group 3 medulloblastoma patient-derived xenografts, Sci. Rep. 8 (2018), doi:10.1038/s41598-018-25263-5.

[53] W. Chen, R.M. Ghobrial, X.C. Li, M. Kloc, Inhibition of RhoA and mTORC2/Rictor by Fingolimod (FTY720) induces p21-activated kinase 1, PAK-1 and amplifies podosomes in mouse peritoneal macrophages, Immunobiology 223 (2018) 634–647, doi:10.1016/j.imbio.2018.07.009.

[54] C. Zhou, M.-.T. Ling, T. Kin-Wah Lee, K. Man, X. Wang, Y.-.C. Wong, FTY720, a fungus metabolite, inhibits invasion ability of androgen-independent prostate cancer cells through inactivation of RhoA-GTPase, Cancer Lett. 233 (2006) 36–47, doi:10.1016/j.canlet.2005.02.039.

[55] Z. Lu, J. Wang, T. Zheng, Y. Liang, D. Yin, R. Song, et al., FTY720 inhibits proliferation and epithelial-mesenchymal transition in cholangiocarcinoma by inactivating STAT3 signaling, BMC Cancer 14 (2014), doi:10.1186/1471-2407-14-783.

[56] L. Zhang, H. Wang, J. Zhu, K. Ding, J. Xu, FTY720 reduces migration and invasion of human glioblastoma cell lines via inhibiting the PI3K/AKT/mTOR/p70S6K signaling pathway, Tumor Biol. 35 (2014) 10707–10714, doi:10.1007/s13277-014-2386-y.
[57] T.K. Lee, FTY720: a promising agent for treatment of metastatic hepatocellular carcinoma, Clin. Cancer Res. 11 (2005) 8458–8466, doi:10.1158/1078-0432.CCR-05-0447.
[58] C.X. Li, Y. Shao, K.T.P. Ng, X.B. Liu, C.C. Ling, Y.Y. Ma, et al., FTY720 suppresses liver tumor metastasis by reducing the population of circulating endothelial progenitor cells, PLoS One 7 (2012), doi:10.1371/journal.pone.0032380.
[59] F.V. Pereira, D.C. Arruda, C.R. Figueiredo, M.H. Massaoka, A.L. Matsuo, V. Bueno, et al., FTY720 induces apoptosis in B16F10-NEX2 murine melanoma cells, limits metastatic development in vivo, and modulates the immune system, Clinics (Sao Paulo) 68 (2013) 1018, doi:10.6061/clinics/2013(07)21.
[60] M.H. Spitzer, Y. Carmi, N.E. Reticker-Flynn, S.S. Kwek, D. Madhireddy, M.M. Martins, et al., Systemic immunity is required for effective cancer immunotherapy, Cell 168 (2017) 487–502 e15, doi:10.1016/j.cell.2016.12.022.
[61] M. Vishnoi, N.H. Liu, W. Yin, D. Boral, A. Scamardo, D. Hong, et al., The identification of a TNBC liver metastasis gene signature by sequential CTC-xenograft modeling, Mol. Oncol. 13 (2019) 1913–1926, doi:10.1002/1878-0261.12533.
[62] E. Koedoot, M. Fokkelman, V.-.M. Rogkoti, M. Smid, I.van de Sandt, H de Bont, et al., Uncovering the signaling landscape controlling breast cancer cell migration identifies novel metastasis driver genes, Nat. Commun. 10 (2019) 1–16, doi:10.1038/s41467-019-11020-3.
[63] W. Chen, A.D. Hoffmann, H. Liu, X. Liu, Organotropism: new insights into molecular mechanisms of breast cancer metastasis, NPJ Precis. Oncol. 2 (2018), doi:10.1038/s41698-018-0047-0.
[64] L.M. Tseng, N.C. Hsu, S.C. Chen, Y.S. Lu, C.H. Lin, D.Y. Chang, et al., Distant metastasis in triple-negative breast cancer, Neoplasma 60 (2013) 290–294, doi:10.4149/neo_2013_038.
[65] K. Beider, E. Rosenberg, H. Bitner, A. Shimoni, M. Leiba, M. Koren-Michowitz, et al., The sphingosine-1-phosphate modulator FTY720 targets multiple myeloma via the CXCR4/CXCL12 pathway, Clin. Cancer Res. 23 (2017) 1733–1747, doi:10.1158/1078-0432.CCR-15-2618.
[66] M.M. Herrmann, S. Barth, B. Greve, K.M. Schumann, A. Bartels, R. Weissert, Identification of gene expression patterns crucially involved in experimental autoimmune encephalomyelitis and multiple sclerosis, Dis. Model. Mech. 9 (2016) 1211–1220, doi:10.1242/dmm.025536.
[67] R.M. Allam, A.M. Al-Abd, A. Khedr, O.A. Sharaf, S.M. Nofal, A.E. Khalifa, et al., Fingolimod interrupts the cross talk between estrogen metabolism and sphingolipid metabolism within prostate cancer cells, Toxicol. Lett. 291 (2018) 77–85, doi:10.1016/j.toxlet.2018.04.008.
[68] Y. Fujimoto, H. Ozawa, T. Higuchi, Y. Miyagawa, A. Bun, M. Imamura, et al., Improved prognosis of low baseline neutrophil-to-lymphocyte ratio is significantly exclusive in breast cancer patients with high absolute counts of lymphocytes, Mol. Clin. Oncol. 10 (2019) 275–284, doi:10.3892/mco.2018.1783.
[69] W. Zhao, P. Wang, H. Jia, M. Chen, X. Gu, M. Liu, et al., Lymphocyte count or percentage: which can better predict the prognosis of advanced cancer patients following palliative care? BMC Cancer 17 (2017) 514, doi:10.1186/s12885-017-3498-8.
[70] S. Spranger, H.K. Koblish, B. Horton, P.A. Scherle, R. Newton, T.F. Gajewski, Mechanism of tumor rejection with doublets of CTLA-4, PD-1/PD-L1, or IDO blockade involves restored IL-2 production and proliferation of CD8+ T cells directly within the tumor microenvironment, J. Immunother. Cancer 2 (2014) 3, doi:10.1186/2051-1426-2-3.
[71] N. Snelder, B.A. Ploeger, O. Luttringer, D.R. Stanski, M. Danhof, Translational pharmacokinetic modeling of fingolimod (FTY720) as a paradigm compound subject to sphingosine kinase-mediated phosphorylation, Drug Metab. Dispos. 42 (2014) 1367–1378, doi:10.1124/dmd.113.056770.
[72] R. Nirogi, N.P. Padala, D.R. Ajjala, R.K. Boggavarapu, P. Kunduru, Incurred sample reanalysis of fingolimod and fingolimod phosphate in blood: stability evaluation and application to a rat pharmacokinetic study, Bioanalysis 9 (2017) 565–577, doi:10.4155/bio-2016-0308.
[73] J.M. Kovarik, R. Schmouder, D. Barilla, G.-.J. Riviere, Y. Wang, T. Hunt, Multiple-Dose FTY720: tolerability, pharmacokinetics, and lymphocyte responses in healthy subjects, J. Clin. Pharmacol. 44 (2004) 532, doi:10.1177/0091270004264165.
[74] Center for Drug Evaluation and Research [CDER]. Application number: 22-527. Clinical pharmacology and biopharmaceutics review(s) [online]. Available from URL: http://www.accessdata.fda.gov/drugsatfda_docs/nda/2010/022527Orig1s000clinpharmr.pdf [Accessed 2020 Nov 8] n.d.
[75] J.-.Y. Wu, Z.-.X. Wang, G. Zhang, X. Lu, G.-.H. Qiang, W. Hu, et al., Targeted co-delivery of Beclin 1 siRNA and FTY720 to hepatocellular carcinoma by calcium phosphate nanoparticles for enhanced anticancer efficacy, Int. J. Nanomed. 13 (2018) 1265–1280, doi:10.2147/IJN.S156328.
[76] L. Galluzzi, L. Senovilla, I. Vitale, J. Michels, I. Martins, O. Kepp, et al., Molecular mechanisms of cisplatin resistance, Oncogene 31 (2012) 1869–1883, doi:10.1038/onc.2011.384.
[77] T. Anasamy, C.F. Chee, L.V. Kiew, L.Y. Chung, In vivo antitumour properties of tribenzyltin carboxylates in a 4T1 murine metastatic mammary tumour model: enhanced efficacy by PLGA nanoparticles, Eur. J. Pharm. Sci. 142 (2020) 105140, doi:10.1016/j.ejps.2019.105140.
[78] B. Feng, Z. Xu, F. Zhou, H. Yu, Q. Sun, D. Wang, et al., Near infrared light-actuated gold nanorods with cisplatin-polypeptide wrapping for targeted therapy of triple negative breast cancer, Nanoscale 7 (2015) 14854–14864, doi:10.1039/c5nr03693c.
[79] F. Yoshii, Y. Moriya, T. Ohnuki, M. Ryo, W. Takahashi, Neurological safety of fingolimod: an updated review, Clin. Exp. Neuroimmunol. 8 (2017) 233–243, doi:10.1111/cen3.12397.
[80] N.C. Hait, D. Avni, A. Yamada, M. Nagahashi, T. Aoyagi, H. Aoki, et al., The phosphorylated prodrug FTY720 is a histone deacetylase inhibitor that reactivates ERα expression and enhances hormonal therapy for breast cancer, Oncogenesis 4 (2015) e156, doi:10.1038/oncsis.2015.16.